Medical Engineering and Physics 115 (2023) 103973

Contents lists available at ScienceDirect

Medical Engineering and Physics

journal homepage: www.elsevier.com/locate/medengphy

Characterization and modeling of the in-plane collagen fiber distribution in the porcine dermis

Suman Jaiswal [a], Rama Hannineh [b], Siva Nadimpalli [c], Samuel Lieber [d], Shawn A. Chester [a,*]

[a] Department of Mechanical Engineering, New Jersey Institute of Technology, Newark, NJ 07102, USA
[b] Department of Biomedical Engineering, New Jersey Institute of Technology, Newark, NJ 07102, USA
[c] Department of Mechanical Engineering, Michigan State University, East Lansing, MI 48824, USA
[d] School of Applied Engineering and Technology, New Jersey Institute of Technology, Newark, NJ 07102, USA

ARTICLE INFO

Keywords:
Anisotropic
Porcine dermis
Collagen
Histology
Non-symmetric distribution
Tissue

ABSTRACT

The structural arrangement of collagen fibers in the plane of the dermis layer plays a critical role in accurately predicting the mechanical behavior of skin tissues. This paper combines a histological analysis with statistical modeling to characterize and model the in-plane collagen fiber distribution in the porcine dermis. The histology data reveals that the fiber distribution in the plane of the porcine dermis is non-symmetric. The histology data forms the basis of our model, which employs a combination of two π-periodic von-Mises distribution density functions to create a non-symmetric distribution. We demonstrate that a non-symmetric in-plane fiber distribution is a significant improvement over a symmetric distribution

1. Introduction

Skin tissues have been widely used in various fields and have found great success in many biomechanical products [1] and medical applications, such as meshes for hernia repair [2] and breast reconstruction [3]. To improve the quality of such products, it is essential to have better insight into the factors affecting the mechanical behavior of skin tissues.

Collagen fibers are one of the most important physical components affecting the mechanical behavior of many soft biological tissues. In particular, the structural arrangement of the collagen fibers significantly impact the mechanical behavior of soft biological tissues. Accordingly, the distribution of the collagen plays a critical role in continuum-level constitutive models for these materials [4–10]. Consequently, to better inform continuum-level constitutive models, an accurate characterization of the structural arrangement of the collagen fibers, which includes both orientation and dispersion, is a significant contribution to constitutive model accuracy.

In this work, we use porcine skin as representative of other soft biological tissues because the fat-free dry weight of skin is composed of 77% of collagen [11], and the methodology developed for skin tissue can be useful and applied to other tissues where collagen fibers are the main mechanical contributor. Further, porcine has similar mechanical characteristics as the human dermis [12] and is found in larger sizes, consequently preferred for various biomedical applications [13].

Typical skin tissues are composed of three major layers: i) the epidermis, the outermost layer; ii) the dermis, the middle layer; and iii) the hypodermis, the innermost layer. We specifically focus on the dermis layer to study the mechanics of skin tissues because the dermis is the main mechanical component of the skin and is broadly composed of a ground substance embedded with collagen fibers [14].

As mentioned previously and reported in the literature, the embedded fibers are the predominant mechanical contributors to the soft biological tissue [15–18]. Lanir [19,20] made seminal contributions in the literature related to characterizing the structural arrangement of the collagen fibers in biological tissues and established that the structural arrangement of the embedded fibers is a key factor in determining the accurate mechanical behavior of soft tissues. According to Lanir's work, the tissue structure is defined in terms of fiber orientation only. However, more recent literature indicates that the fibers are also dispersedly oriented [21,22]. Accordingly, many experiments have been conducted to study the collagen fiber distribution in soft biological tissues [cf. e.g., 23–31]. A major broad outcome of all that work indicates that the collagen fibers and their structural arrangement are the vital factors for

* Corresponding author.
E-mail address: shawn.a.chester@njit.edu (S.A. Chester).

https://doi.org/10.1016/j.medengphy.2023.103973
Received 7 December 2022; Received in revised form 6 March 2023; Accepted 28 March 2023
Available online 31 March 2023

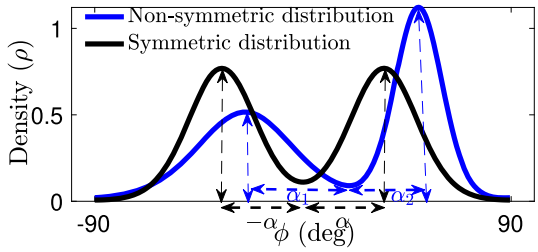

Fig. 1. Schematic of a distribution for two collagen fiber families illustrating a symmetric and a non-symmetric distribution.

characterizing the mechanical behavior and informing continuum-level constitutive models.

Nearly all of the prior literature uses histological analysis, a microscopy-based method used to determine the orientation, distribution, and other details of the collagen fibers. The relevant significant findings from the prior literature may be summarized with just a few main points. i) there are typically two fiber families in the dermis [18,26], ii) the spatial collagen fiber distribution differs between in-plane and out of plane [26,29,9], and iii) the collagen fiber distribution in the plane of the dermis has a more significant effect on the mechanical behavior than the out-of-plane distribution [26].

In the modeling literature related to the structural arrangement of collagen fibers, two common approaches have been established to describe the spatial distribution of collagen fibers within the tissue: i) the angular integration approach [24,32,33]; and ii) the generalized structural tensor approach [4,29]. The angular integration approach considers individual fiber contributions in its material description. Consequently, the angular integration approach gives accurate results, but it is not a viable option for efficient numerical implementation since it requires a large number of calculations [5]. In contrast, the generalized structural tensor approach considers the average of all the fibers in its calculations and therefore is a viable option for numerical implementation since it requires fewer calculations and is amenable for implementation in a finite element environment [27]. For more details about the difference between the angular integration and the generalized structural tensor approach, readers are referred to Holzapfel et al. [30]. Irrespective of the approach employed, the components characterizing the structural arrangement, specifically the mean orientations and measure of fiber dispersion of the embedded fibers, are paramount to the continuum level constitutive model.

It is well known that the true collagen fiber distribution is three-dimensional. However, as reported in the literature, the fiber distribution in the plane of the dermis is more significant than the out-of-plane distribution [26]. Accordingly, this work focuses on characterizing and modeling the collagen fiber distribution in the plane of the porcine dermis, which we experimentally observed to be non-symmetric. Fig. 1 shows a schematic that clarifies the difference between a symmetric fiber distribution and a non-symmetric planar fiber distribution employing the π-periodic von-Mises distribution for two fiber families. As the name suggests, the fibers are symmetrically distributed for a symmetric fiber distribution with two distinct fiber families. In Fig. 1 this is indicated by the equal orientations and identical peak heights and widths. In contrast, the non-symmetric distribution with two fiber families still has two peaks with different heights, widths, and mean orientations.

Focusing on the generalized structure tensor approach to describe the fiber distribution, the main physical quantities are: i) the mean fiber orientation; and ii) the measure of the dispersion from the mean orientation. Within the context of the generalized structural tensor approach, these are termed *structural parameters*, and significant prior literature exists. The most notable work is Gasser et al. [4], where the foundation of this approach originated and was focused on modeling artery walls. Gasser et al. [4] proposed a statistical-based model to characterize the collagen fiber spatial distribution considering the mean orientation and dispersion, assuming transverse isotropy for an arterial wall. A few more seminal contributions are Jor et al. [26], Annaidh et al. [27], Holzapfel et al. [29], Holzapfel et al. [30], Ueda et al. [34] and Witte et al. [7]. Jor et al. [26] focused on characterizing collagen fiber distribution through the thickness of the porcine dermis. Annaidh et al. [27] applied the method of Gasser et al. [4] to skin tissues but mostly kept the underlying model unchanged. More recently, Holzapfel and co-workers [29,30] have enhanced their seminal contribution from Gasser et al. [4], but the in-plane fiber distribution is still assumed to be symmetric. The work of Ueda et al. [34] and Witte et al. [7] have experimentally shown that the human dermis has non-symmetric fiber distribution, but it was not explicitly modeled.

Although a lot has gone into characterizing the structural arrangement of collagen fibers, the existing literature has not yet made use of a non-symmetric planar fiber distribution to characterize and model the fiber distribution in the plane of dermis. Many state-of-the-art constitutive models require the details of the structural arrangement of fibers as input. Accordingly, there is a clear gap in properly informing continuum level constitutive models, which may be improved by using a more physically relevant fiber distribution, i.e., considering the non-symmetry of planar fiber distribution.

Our experimental investigation demonstrates that the fiber distribution in the plane of the dermis is non-symmetric, and accordingly we hypothesize that the in-plane collagen fiber distribution is more accurately described by a non-symmetric model than a symmetric distribution. Accordingly, the objective of this paper is to experimentally characterize and model the collagen fiber distribution in the plane of the dermis. This is accomplished by measuring the collagen fiber distribution in the plane of the porcine dermis through the use of histology analysis and employing a ubiquitously used π-periodic von-Mises distribution model ([4,26,35,29,36]), which is enhanced to capture the non-symmetric planar fiber distribution with two fiber families. The enhanced model is general and should be applicable to any soft biological tissue composed of collagen fibers. Here we use porcine dermis as a representative material.

The remainder of this paper is organized as follows. Section 2 overviews the procedure of sample preparation for histology analysis, including staining and image acquisition, and also describes the details of the modeling approach. Section 3 summarizes the results obtained. 4 discusses the observations of results and the final Section 5 summarizes what is learned from this research and provides some concluding remarks.

2. Materials and methods

The porcine skin tissue used in this work was produced by Midwest Research Swine (Glencoe, MN). Midwest Research Swine has an established quality-controlled process to provide high-quality porcine tissue and live research swine typically used for biomedical applications. The porcine skin was obtained from a six-month male 241 pound American Yorkshire-Landrace-Duroc, the skin was debristled, and the hypodermis was removed per MRS established process [37].

2.1. Sample preparation

We received the skin tissue in the form of rectangular sheets. Fig. 2 shows a schematic of two adjacent tissue sections taken from the left and right of the spine, nearest to the tail, along with our coordinate system. The tissue sheets have notches indicating the head and spine sides to ensure a consistent reference system. Following the approach of [37] after receiving the tissue, the sheets were stored in a freezer at −80 °C to prevent any degradation. Before use, the tissue sheets were defrosted for 24 hours in a 4 °C refrigerator before preparing the histology samples using a custom steel rule die. A custom die allows us to produce histology samples keeping the orientation known with respect to the head and spine. This will ensure that the orientation of the identified

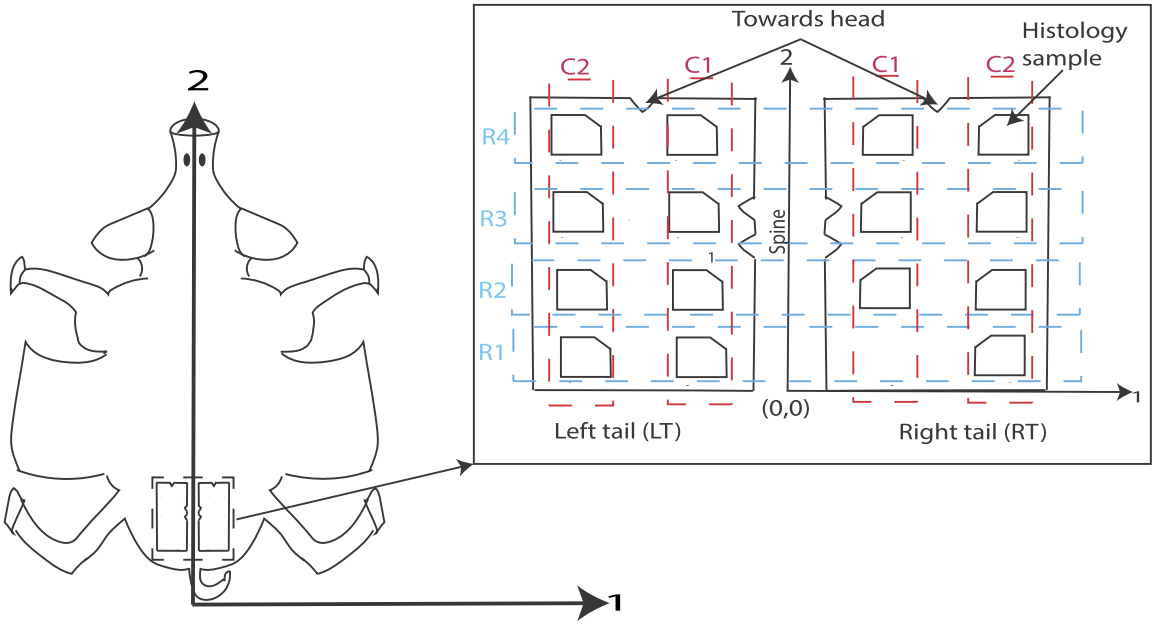

Fig. 2. Schematic of two sections of porcine dermis showing the various locations from where the fifteen histology samples were taken. The approximate size of each section is 300 mm × 450 mm. The image is not drawn to scale.

collagen fibers can then be measured relative to the head and spine as references.

The schematic in Fig. 2 also shows various locations labeled as rows and columns, which we use to indicate where the samples for histology analysis have been extracted from the sheet. In our convention, columns closer to the spine are labeled C1, and the columns further from the spine are labeled C2. And rows nearest to the tail are labeled as R1 and continue to increase, moving upward towards the head. The coordinates of the locations marked as rows and columns have been determined to have a physical sense of length scale. We have used ImageJ software [38] to obtain the coordinates of the locations labeled using our row-column convention. The coordinates represent the center position of each location, taking the end of the spine towards the tail as the reference.

The die-cut tissue samples were then placed in individual histology cassettes to keep proper track of the locations. We followed the established procedure for the histology analysis used at the New Jersey Medical School, an institution affiliated with and neighboring NJIT. Cassettes containing samples were fixed in 10% neutral buffered Formalin [39,40] for 24 hours followed by storage in 70% Ethanol [41] and sent for histology analysis.

2.2. Histology imaging

Histology samples were processed at the New Jersey Medical School. The hypodermis side of the tissue sample was faced, and imaging was done at 300 microns deep from the hypodermis side to ensure that the histology samples were taken from the dermis layer. We have used a well-established method to identify the collagen bundles in the dermis by employing the picrosirius red stain [42,43,40]. A Nikon Eclipse microscope was employed under polarized light using a Nikon Plan Apo 4× objective with numerical aperture of 0.2, and the 4× images were stitched together to view the full tissue histology sample of 9.5 mm × 9.5 mm. Representative images of samples from both the left and the right of the spine are shown in Fig. 3.

A limitation of our work, is that the imaging for the collagen fiber distributions was performed post mortem. And this may affect the macroscopic dimensions of the tissue as well as the microscopic collagen fiber distribution due to loss of residual stress or pre-tension among other factors [44]. We believe that more accurate fiber distributions may be measured if the data were obtained *in vivo*, however that is outside the scope of our work in this contribution.

2.3. Obtaining individual fiber orientations

To obtain the planar fiber orientations, we employ OrientationJ vector field, a plugin of ImageJ [38]. The software uses an image-based region of interest to obtain the fiber orientations utilizing the coordinate system shown in Fig. 2.

The collagen fibers in the dermis are predominantly oriented along cleavage lines, also known as Langer lines [cf. e.g., 45–47,6, and references therein]. In the porcine dermis, the cleavage lines can be seen as running in a direction transverse to the spine [48,49]. Accordingly, we have taken the transverse to the spine direction as our reference for fiber orientation measurement as shown in Fig. 3b.

Our testing indicates that the results are affected primarily by the size of the region of interest, the so-called σ parameter in OrientationJ vector field. Accordingly, in order to determine an appropriate value for σ, a convergence study was conducted on the fiber orientations. Based on the mean orientation results shown in Fig. 4, it can be observed that the mean orientations for both the first fiber family and the second fiber family are converging around $\sigma = 4$, therefore for good measure, all analyses reported here use $\sigma = 6$.

2.4. Models for the fiber distribution

The existing literature almost ubiquitously uses the very common π-periodic von-Mises distribution probability density function. This density function is for the directional statistics for unimodal circular data [4,26,35,29,36]. As it serves as the foundational building block for much of the description of collagen fibers, for clarity it is briefly summarized here. For an angle ϕ, it's given by

$$\rho(\phi) = \left\{ \frac{\exp\left[b\cos 2(\phi-\alpha)\right]}{2\pi I_0(b)} \right\}, \quad -\pi/2 \le \phi \le \pi/2 \tag{2.1}$$

where α is the mean orientation, b is a measure of the fiber concentration, and $I_0(b)$ is the modified Bessel function of the first kind of order zero and defined as

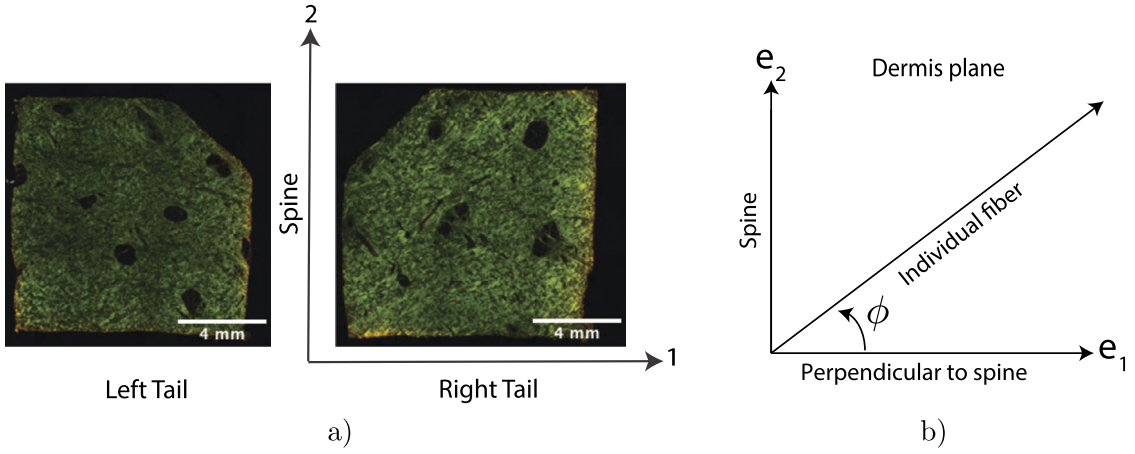

Fig. 3. a) Representative images (each is approximately 9.5 mm × 9.5 mm) of the stained histology samples from the left and right sides of the spine under polarized light, b) Schematic of reference chosen for measurement of fiber orientation.

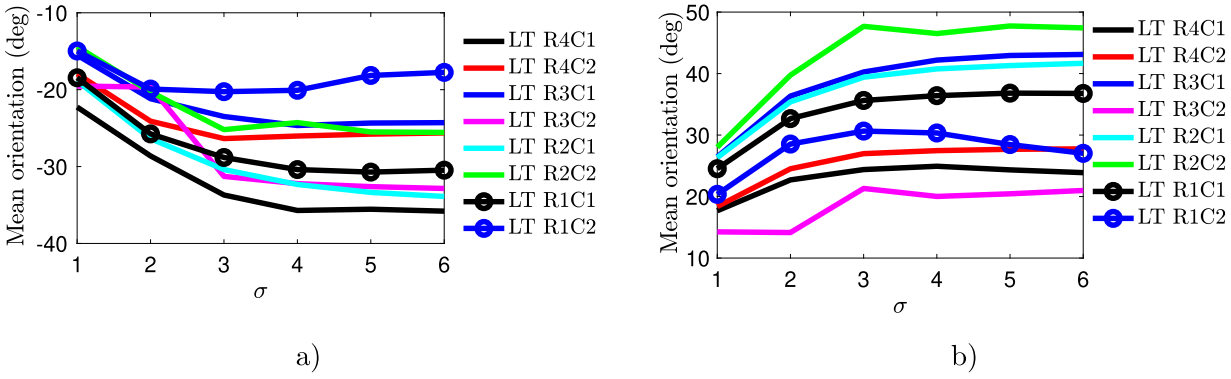

Fig. 4. Results of our convergence study for the parameter σ for the mean orientation of a) the first fiber family, and b) the second fiber family, using a handful of samples from the left tail region.

$$I_0(b) = \frac{1}{\pi}\int_0^{\pi} \exp(b\cos\phi)\, d\phi\,. \tag{2.2}$$

Further, the density distribution function (2.1) must satisfy the following normalization condition

$$\int_{-\pi/2}^{\pi/2} \rho(\phi) d\phi = 1\,. \tag{2.3}$$

To account for two distinct fiber families, as will be shown in what follows, we employ a combination of two π-periodic von-Mises distribution probability density functions for modeling the fiber distribution in the plane of the porcine dermis. As mentioned in Section 1, the existing literature for modeling the fiber distribution considers a symmetric distribution [27,29]. However, our experimental results (see Fig. 5) and others in the literature [34,7] show that the fiber distribution in the plane of the porcine dermis is non-symmetric. Accordingly, we hypothesized that a non-symmetric distribution could more accurately characterize the fiber distribution in the plane of the dermis. Therefore, in this work, building upon the prior modeling literature [4,29], we have enhanced the existing π-periodic von-Mises distribution probability density functions to capture the non-symmetric planar fiber distribution, and it was compared with a well-established symmetric distribution model to test our hypothesis.

2.4.1. Symmetric planar fiber distribution

To give context, we find it useful to first describe the standard symmetric planar fiber distribution. For a symmetric planar distribution of collagen fibers, as shown in Fig. 1, the mean orientations are equal and opposite, and the fiber dispersion for both the fiber families is identical. Consequently, the total probability density function for the in-plane symmetric fiber distribution is given by

$$\rho_{\text{sym}}(\phi) = \left\{ \frac{\exp[b\cos 2(\phi+\alpha)]}{2\pi I_0(b)} + \frac{\exp[b\cos 2(\phi-\alpha)]}{2\pi I_0(b)} \right\}. \tag{2.4}$$

The fiber dispersion for the symmetric distribution is then obtained through

$$\kappa_{\text{sym}} = \int_{-\pi/2}^{\pi/2} \left\{ \frac{\exp(b\cos 2\phi)}{\pi I_0(b)} \right\} \sin^2(\phi) d\phi\,, \quad 0 \le \kappa_{\text{sym}} \le 1/2\,, \tag{2.5}$$

and the normalization condition for symmetric fiber distribution is given by

$$\int_{-\pi/2}^{\pi/2} \rho_{\text{sym}}(\phi) d\phi = \int_{-\pi/2}^{\pi/2} \left\{ \frac{\exp[b\cos 2(\phi+\alpha)]}{2\pi I_0(b)} + \frac{\exp[b\cos 2(\phi-\alpha)]}{2\pi I_0(b)} \right\} d\phi = 1\,. \tag{2.6}$$

2.4.2. Non-symmetric planar fiber distribution

For a non-symmetric planar fiber distribution, as shown in Fig. 1 and the foundation of our hypothesis, both fiber families have distinct mean orientations and dispersions, with the total probability density function given by

$$\rho_{\text{non-sym}}(\phi) = \left\{ \frac{\exp[b_1\cos 2(\phi-\alpha_1)]}{2\pi I_0(b_1)} + \frac{\exp[b_2\cos 2(\phi-\alpha_2)]}{2\pi I_0(b_2)} \right\}, \tag{2.7}$$

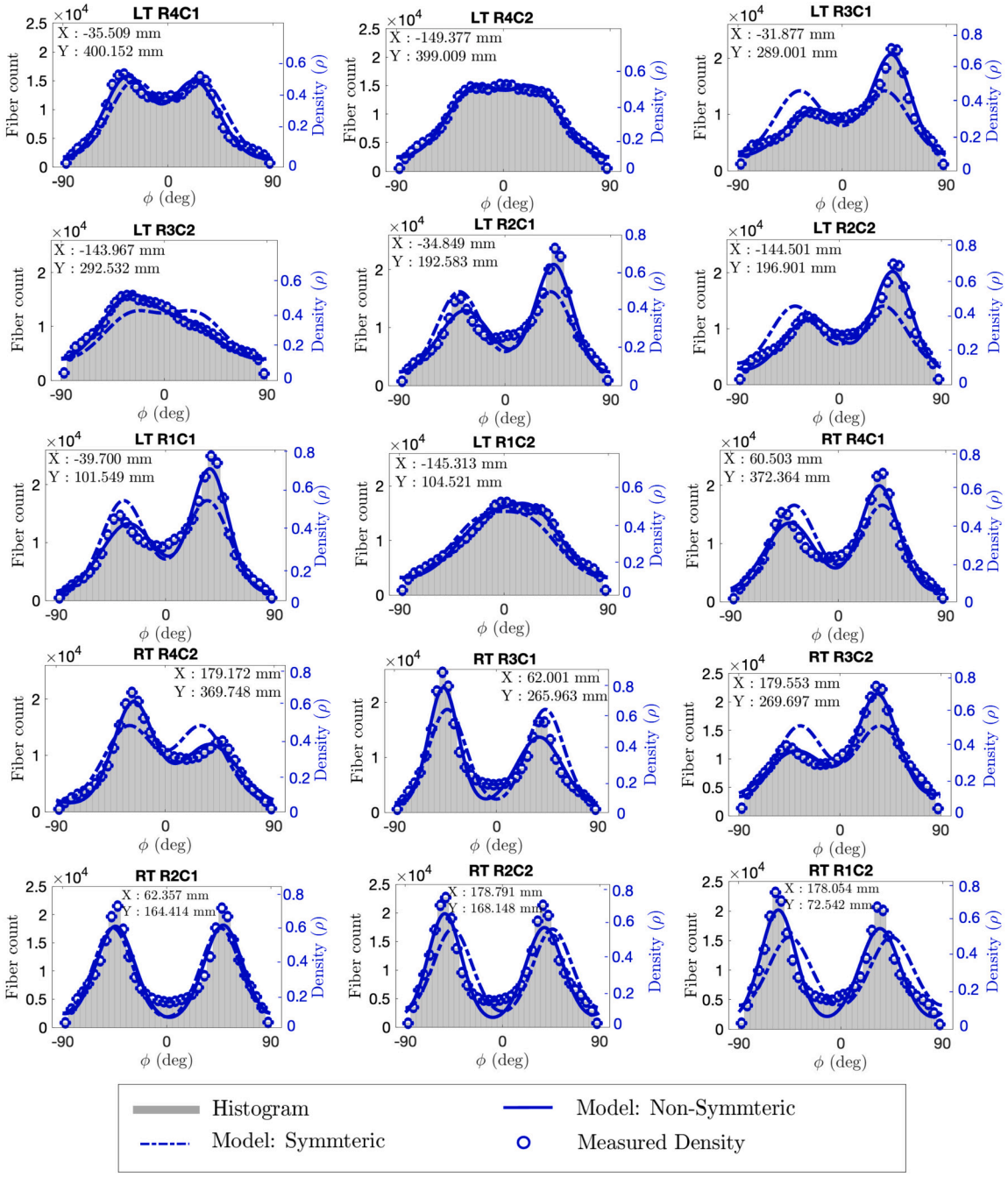

Fig. 5. Histogram of measured fiber counts from histological analysis for all locations. Superimposed are the measured fiber density, as well as the calibrated non-symmetric and symmetric models.

where α_1 and b_1 are the mean orientation and concentration, respectively for the first fiber family, and α_2 and b_2 are the same for the second fiber family. Further, the fiber dispersion for each fiber family can be obtained from

$$\kappa_1 = \int_{-\pi/2}^{\pi/2} \left\{ \frac{\exp(b_1 \cos 2\phi)}{\pi I_0(b_1)} \right\} \sin^2(\phi) d\phi, \quad \text{and}$$

$$\kappa_2 = \int_{-\pi/2}^{\pi/2} \left\{ \frac{\exp(b_2 \cos 2\phi)}{\pi I_0(b_2)} \right\} \sin^2(\phi) d\phi, \tag{2.8}$$

where $0 \le \kappa_1 \le 1/2$, and $0 \le \kappa_2 \le 1/2$. And the normalization condition for non-symmetric distribution is given by

$$\int_{-\pi/2}^{\pi/2} \left\{ \frac{\exp[b_1 \cos 2(\phi - \alpha_1)]}{2\pi I_0(b_1)} + \frac{\exp[b_2 \cos 2(\phi - \alpha_2)]}{2\pi I_0(b_2)} \right\} d\phi = 1\,. \tag{2.9}$$

Employing the normalization condition given by equation (2.9) is equivalent to using different weights to two sets of fiber families.

3. Results

As mentioned in Section 2.1, we have fifteen histology samples from the various locations of the porcine dermis in the vicinity of the tail, as indicated in Fig. 2. Using the methods described in Sections 2.2 and 2.3, the planar fiber orientations were obtained and analyzed. The planar fiber orientations obtained from each histology sample are plotted as histograms with 5° bin intervals as shown in Fig. 5. These histograms

Table 1
List of structural parameters obtained by calibration of a model consisting of a combination of two von-Mises distributions with the planar fiber orientations considering various locations with respect to the spine employing both the symmetric distribution and non-symmetric distribution approach.

Location	Coordinates (mm)	Symmetric		Non-symmetric			
		α	κ_{sym}	α_1	α_2	κ_1	κ_2
LT R4C1	X: -35.509 Y: 400.152	29.85°	0.165	−35.8°	23.89°	0.147	0.159
LT R4C2	X: -149.377 Y: 399.009	26.67°	0.206	−25.63°	27.75°	0.203	0.208
LT R3C1	X: -31.877 Y: 289.001	37.21°	0.181	−24.29°	43.11°	0.264	0.102
LT R3C2	X: -143.967 Y: 292.532	29.19°	0.260	−32.85°	21.0°	0.217	0.317
LT R2C1	X: -34.849 Y: 192.583	38.80°	0.139	−33.89°	41.67°	0.207	0.0923
LT R2C2	X: -144.501 Y: 196.901	39.42°	0.186	−25.55°	47.43°	0.235	0.102
LT R1C1	X: -39.700 Y:101.549	34.71°	0.123	−30.47°	36.77°	0.199	0.078
LT R1C2	X: -145.313 Y: 104.521	22.96°	0.254	−17.75°	27.03°	0.271	0.232
RT R4C1	X: 60.503 Y: 372.364	37.12°	0.133	−40.50°	34.60°	0.181	0.091
RT R4C2	X: 179.172 Y: 369.748	30.70°	0.160	−26.53°	37.41°	0.095	0.210
RT R3C1	X: 62.001 Y: 265.963	43.38°	0.099	−46.82°	37.94°	0.058	0.157
RT R3C2	X: 179.553 Y: 269.697	36.13°	0.181	−38.99°	33.88°	0.278	0.116
RT R2C1	X: 62.357 Y: 164.414	46.50°	0.104	−44.25°	48.80°	0.102	0.100
RT R2C2	X: 178.791 Y: 168.148	46.21°	0.123	−53.48°	38.80°	0.085	0.110
RT R1C2	X: 178.054 Y: 72.542	44.93°	0.149	−55.11°	34.68°	0.0848	0.119

LT: Left Tail; RT: Right Tail.

represent the number of fibers oriented along different directions. The fiber counts were also converted into experimentally measured fiber density, ensuring that the normalization condition given by (2.9) is satisfied for each sample. The experimentally measured fiber density is superimposed on the histograms in Fig. 5. From the experimental measurements shown in Fig. 5 one may clearly observe that, in general, the actual fiber distribution is non-symmetric, and thus a model considering the non-symmetric fiber distribution will better capture the actual fiber distribution as compared to a model that considers only symmetric distribution ubiquitously found in the literature. The prior literature based on the symmetric fiber distribution (2.4), and the enhanced model considering the non-symmetric fiber distribution (2.7), are calibrated using the least-squares method to the measured distribution and are superimposed on the histograms in Fig. 5 as lines.

4. Discussion

In Fig. 5 the solid lines represent the non-symmetric distribution, and the dash-dot lines indicate the symmetric planar fiber distribution. As expected, it is clear from the Fig. 5 that the non-symmetric fiber distribution modeled through (2.7) more accurately characterizes the structural arrangement of the collagen fibers than the symmetric distribution model. Table 1 provides the specific parameter values for the mean orientations and dispersion of the fiber distributions obtained from calibration for both the models.

Further, to evaluate the predictive quality of both models, we have calculated the Root Mean Square Error (RMSE) and the R^2 (also known as “goodness of fit”) for both the symmetric and non-symmetric models. Fig. 6 is a box-plot that shows that the non-symmetric model is superior to the symmetric model for this data set. For completeness, Table 2 summarizes the values of RMSE for both the models. It can be noticed that the error caused by employing symmetric distribution is more than the non-symmetric distribution in all cases, with improvements as large as 200% achieved through the use of the new non-symmetric distribution. Additionally, Table 3 provides the tabulated comparison between the symmetric and non-symmetric distributions by using R^2. Again, it is clear that the non-symmetric distribution shows a considerable improvement over the symmetric distribution in all cases. In three cases, RT R1C2, LT R2C2, and LT R3C1, the improvement in terms of R^2 values demonstrated by the non-symmetric distribution approach is more than 70%, a remarkably significant improvement.

5. Conclusion

We have experimentally demonstrated that the fiber distribution in the plane of the porcine dermis is generally non-symmetric with two sets of fiber families. This was accomplished by experimentally measur-

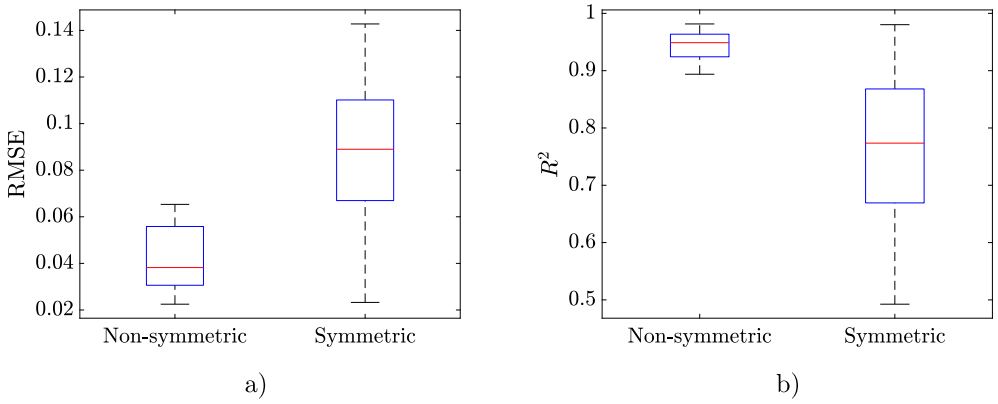

Fig. 6. Box-plots showing the comparison of symmetric and non-symmetric distribution in terms of a) Root Mean Square Error (RMSE), and b) R^2.

Table 2
Summary of RMSE values for symmetric and non-symmetric approach demonstrating a significant reduction in root mean square error by non-symmetric method over symmetric method while capturing the real fiber orientation.

Location	Coordinates (mm)	Symmetric, RMSE	Non-symmetric, RMSE	% difference in RMSE values
LT R3C1	X: -31.877 Y: 289.001	0.1128	0.0365	209.20%
LT R2C2	X: -144.501 Y: 196.901	0.1114	0.0382	191.67%
RT R3C2	X: 179.553 Y: 269.697	0.0900	0.0324	178.02%
RT R4C2	X: 179.172 Y: 369.748	0.0927	0.0355	160.96%
LT R3C2	X: -143.967 Y: 292.532	0.0685	0.0278	145.99%
RT R1C2	X: 178.054 Y: 72.5424	0.1428	0.0653	118.56%
RT R2C2	X:178.791 Y: 168.148	0.1172	0.0587	99.76%
LT R1C1	X: -39.700 Y:101.549	0.0890	0.0461	92.84%
LT R4C1	X: -35.509 Y: 400.152	0.0577	0.0300	92.25%
RT R3C1	X: 62.001 Y: 265.963	0.1063	0.0597	78.11%
LT R1C2	X: -145.313 Y: 104.521	0.0479	0.0276	73.37%
RT R4C1	X: 60.503 Y: 372.364	0.0813	0.0473	71.94%
LT R2C1	X: -34.849 Y: 192.583	0.0847	0.0495	71.13%
RT R2C1	X: 62.357 Y: 164.414	0.0665	0.0580	14.66%
LT R4C2	X: - 149.377 Y: 399.009	0.0232	0.0225	3.39%

LT: Left Tail; RT: Right Tail.

Table 3
Summary of R^2 values for symmetric and non-symmetric approach demonstrating a significant improvement by non-symmetric method over symmetric method while capturing the real fiber orientation.

Location	Coordinates (mm)	Symmetric, R^2	Non-symmetric, R^2	% improvement
RT R1C2	X: 178.054 Y: 72.542	0.493	0.894	81.3%
LT R2C2	X: -144.501 Y: 196.901	0.528	0.945	79.0%
LT R3C1	X: -31.877 Y: 289.001	0.557	0.954	71.3%
RT R3C2	X: 179.553 Y: 269.697	0.669	0.957	43.0%
RT R2C2	X: 178.791 Y: 168.148	0.671	0.918	36.8%
LT R3C2	X: -143.967 Y: 292.532	0.749	0.959	28.0%
RT R4C2	X: 179.172 Y: 369.748	0.764	0.965	26.3%
RT R3C1	X: 62.001 Y: 265.963	0.774	0.929	20.0%
LT R2C1	X: -34.849 Y: 192.583	0.774	0.923	19.3%
LT R1C1	X: -39.700 Y: 101.549	0.810	0.949	17.16%
RT R4C1	X: 60.503 Y: 372.364	0.807	0.935	15.9%
LT R4C1	X: -35.509 Y: 400.152	0.895	0.972	8.6%
LT R1C2	X: -145.313 Y: 104.521	0.914	0.971	6.2%
RT R2C1	X: 62.357 Y: 164.414	0.888	0.914	3.0%
LT R4C2	X: -149.377 Y: 399.009	0.980	0.982	0.2%

LT: Left Tail; RT: Right Tail.

ing the orientations of collagen fibers in the plane of the porcine dermis using histology analysis. Based on the histology data, we have developed and verified an enhanced statistical-based model that considers the non-symmetry of the fiber distribution by employing a combination of two π-periodic von-Mises distribution density functions.

The main novelty of this work is experimentally demonstrating that a non-symmetric in-plane fiber distribution model more accurately captures the collagen distribution of real tissue and does so without any additional experimental or computational effort in terms of cost and time when compared with the ubiquitous symmetric distribution. Further, we expect our method to easily extend to all soft biological tissues since almost all soft biological tissues consist of collagen fibers in a softer matrix.

We believe this work has far-reaching implications for structure-based continuum level constitutive models that make use of the structural arrangement of fibers as input. The improvements shown here using our non-symmetric model, when used as part of a simulation tool, can lead to the development of new and improved devices and applications, which may impact many lives. While much was learned in this work, there is still much to be done. Future studies aim to characterize the effect of aging and gender on the collagen fiber microstructure in the porcine dermis.

Declarations

Ethical approval: Not required. Funding: SAC acknowledges partial support from the National Science Foundation under grant numbers (CMMI-1463121) and (CMMI-1751520). SN acknowledges partial support from the National Science Foundation under grant numbers (CMMI-1652409) and (CMMI-2026717).

Declaration of competing interest

Competing interests: None.

Acknowledgements

SAC acknowledges partial support from the National Science Foundation under grant numbers (CMMI-1463121) and (CMMI-1751520). SN acknowledges partial support from the National Science Foundation under grant numbers (CMMI-1652409) and (CMMI-2026717). The opinions, findings, and conclusions, or recommendations expressed are those of the author(s) and do not necessarily reflect the views of the National Science Foundation. The authors would like to thank Midwest Research Swine, LLC for providing the material for the testing. The authors would also like to thank Luke Fritzky, Cellular Imaging and Histology Core, NJMS Cancer Center NJ for histology imaging on the porcine dermis samples.

Appendix A. Supplementary material

Supplementary material related to this article can be found online at https://doi.org/10.1016/j.medengphy.2023.103973.

References

[1] Wood Garrett W, Panzer Matthew B, Bass Cameron R, Myers Barry S. Viscoelastic properties of hybrid iii head skin. SAE Int J Mater Manuf 2010;3(1):186–93. ISSN 19463979, 19463987. http://www.jstor.org/stable/26282897.

[2] Rastegarpour Ali, Cheung Michael, Vardhan Madhurima, Ibrahim Mohamed M, Butler Charles E, Levinson Howard. Surgical mesh for ventral incisional hernia repairs: understanding mesh design. Plast Surg 2016;24(1):41–50.

[3] Logan Ellis Hugh, Asaolu Oluwatosin, Nebo Vivien, Kasem Abdul. Biological and synthetic mesh use in breast reconstructive surgery: a literature review. World J Surg Oncol 2016;14(1):1–9.

[4] Gasser T Christian, Ogden Ray W, Holzapfel Gerhard A. Hyperelastic modelling of arterial layers with distributed collagen fibre orientations. J R Soc Interface 2006;3(6):15–35. https://doi.org/10.1098/rsif.2005.0073. ISSN 17425662.

[5] Cortes Daniel H, Lake Spencer P, Kadlowec Jennifer A, Soslowsky Louis J, Elliott Dawn M. Characterizing the mechanical contribution of fiber angular distribution in connective tissue: comparison of two modeling approaches. Biomech Model Mechanobiol 2010;9(5):651–8. https://doi.org/10.1007/s10237-010-0194-x. ISSN 16177959.

[6] Hamed Joodaki, Panzer Matthew B. Skin mechanical properties and modeling: a review. Proc Inst Mech Eng, H J Eng Med 2018;232(4):323–43. https://doi.org/10.1177/0954411918759801. PMID: 29506427.

[7] Witte Maximilian, Jaspers Sören, Wenck Horst, Rübhausen Michael, Fischer Frank. General method for classification of fiber families in fiber-reinforced materials: application to in-vivo human skin images. Sci Rep 2020;10(1):1–11.

[8] Meador William D, Sugerman Gabriella P, Story Hannah M, Seifert Ashley W, Bersi Matthew R, Tepole Adrian B, et al. The regional-dependent biaxial behavior of young and aged mouse skin: a detailed histomechanical characterization, residual strain analysis, and constitutive model. Acta Biomater 2020;101:403–13.

[9] Sadeghinia Mohammad Javad, Skallerud Bjørn, Holzapfel Gerhard A, Prot Victorien. Biomechanics of mitral valve leaflets: second harmonic generation microscopy, biaxial mechanical tests and tissue modeling. Acta Biomater 2022;141:244–54.

[10] Han Hai-Chao. Effects of material non-symmetry on the mechanical behavior of arterial wall. J Mech Behav Biomed Mater 2022;129:105157.

[11] Weinstein GD, Boucek RJ. Collagen and elastin of human dermis. J Invest Dermatol 1960;35(4):227–9. https://doi.org/10.1038/jid.1960.109. ISSN 0022202X.

[12] Shergold Oliver A, Fleck Norman A, Radford Darren. The uniaxial stress versus strain response of pig skin and silicone rubber at low and high strain rates. Int J Impact Eng 2006;32(9):1384–402. https://doi.org/10.1016/j.ijimpeng.2004.11.010. ISSN 0734743X.

[13] Swindle MM, Makin A, Herron AJ, Clubb FJ, Frazier KS. Swine as models in biomedical research and toxicology testing. Vet Pathol 2012;49(2):344–56. https://doi.org/10.1177/0300985811402846. ISSN 15442217.

[14] Benítez José María, Montáns Francisco Javier. The mechanical behavior of skin: structures and models for the finite element analysis. Comput Struct 2017;190:75–107. https://doi.org/10.1016/j.compstruc.2017.05.003. ISSN 00457949.

[15] Craik JE, Mcneil IRR. 14 - Histological studies of stressed skin. In: Kenedi RM, editor. Biomechanics and related bio-engineering topics. Pergamon. ISBN 978-1-4831-6701-5, 1965. p. 159–64.

[16] Brown Ia. Scanning electron microscopy of human dermal fibrous tissue. J Anat 1972;113:159–68.

[17] Lanir Y, Fung YC. Two-dimensional mechanical properties of rabbit skin—ii. Experimental results. J Biomech 1974;7(2):171–82.

[18] Meyer W, Neurand K, Radke B. Collagen fibre arrangement in the skin of the pig. J Anat 1982;134(1):139–48.

[19] Lanir Y. A structural theory for the homogeneous biaxial stress-strain relationships in flat collagenous tissues. J Biomech 1979;12(6):423–36.

[20] Lanir Yan. Constitutive equations for fibrous connective tissues. J Biomech 1983;16(1):1–12.

[21] Canham Peter B, Finlay Helen M, Dixon Jan G, Boughner Derek R, Chen Andrew. Measurements from light and polarised light microscopy of human coronary arteries fixed at distending pressure. Cardiovasc Res 1989;23(11):973–82. https://doi.org/10.1093/cvr/23.11.973. ISSN 00086363.

[22] Finlay Helen M, Whittaker Peter, Canham Peter B. Collagen organization in the branching region of human brain arteries. Stroke 1998;29(8):1595–601. https://doi.org/10.1161/01.STR.29.8.1595. ISSN 00392499.

[23] Noorlander Maril L, Melis Paris, Jonker Ard, Van Noorden Cornelis JF. A quantitative method to determine the orientation of collagen fibers in the dermis. J Histochem Cytochem 2002;50(11):1469–74.

[24] Sacks Michael S. Incorporation of experimentally-derived fiber orientation into a structural constitutive model for planar collagenous tissues. J Biomech Eng 2003;125(2):280–7. https://doi.org/10.1115/1.1544508. ISSN 01480731.

[25] Sander Edward A, Stylianopoulos Triantafyllos, Tranquillo Robert T, Barocas Victor H. Image-based biomechanics of collagen-based tissue equivalents. IEEE Eng Med Biol Mag 2009;28(3):10–8.

[26] Jor Jessica WY, Nielsen Poul MF, Nash Martyn P, Hunter Peter J. Modelling collagen fibre orientation in porcine skin based upon confocal laser scanning microscopy. Skin Res Technol 2011;17(2):149–59.

[27] Annaidh Aisling Ni, Bruyère Karine, Destrade Michel, Gilchrist Michael D, Maurini Corrado, Otténio Melanie, et al. Automated estimation of collagen fibre dispersion in the dermis and its contribution to the anisotropic behaviour of skin. Ann Biomed Eng 2012;40(8):1666–78. https://doi.org/10.1007/s10439-012-0542-3. ISSN 00906964.

[28] Schriefl Andreas J, Zeindlinger Georg, Pierce David M, Regitnig Peter, Holzapfel Gerhard A. Determination of the layer-specific distributed collagen fibre orientations in human thoracic and abdominal aortas and common iliac arteries. J R Soc Interface 2012;9(71):1275–86.

[29] Holzapfel Gerhard A, Niestrawska Justyna A, Ogden Ray W, Reinisch Andreas J, Schriefl Andreas J. Modelling non-symmetric collagen fibre dispersion in arterial walls. J R Soc Interface 2015;12(106):20150188.

[30] Holzapfel Gerhard A, Ogden Ray W, Sherifova Selda. On fibre dispersion modelling of soft biological tissues: a review. Proc R Soc A, Math Phys Eng Sci 2019;475(2224). https://doi.org/10.1098/rspa.2018.0736. ISSN 14712946.

[31] Jadidi Majid, Sherifova Selda, Sommer Gerhard, Kamenskiy Alexey, Holzapfel Gerhard A. Constitutive modeling using structural information on collagen fiber direction and dispersion in human superficial femoral artery specimens of different ages. Acta Biomater 2021;121:461–74.

[32] Driessen Niels JB, Bouten Carlijn VC, Baaijens Frank PT. A structural constitutive model for collagenous cardiovascular tissues incorporating the angular fiber distribution. J Biomech Eng 2005;127(3):494–503. https://doi.org/10.1115/1.1894373. ISSN 01480731.

[33] Ateshian Gerard A, Rajan Vikram, Chahine Nadeen O, Canal Clare E, Hung Clark T. Modeling the matrix of articular cartilage using a continuous fiber angular distribution predicts many observed phenomena. J Biomech Eng 2009;131(6):1–10. https://doi.org/10.1115/1.3118773. ISSN 01480731.

[34] Ueda Maho, Saito Susumu, Murata Teruasa, Hirano Tomoko, Bise Ryoma, Kabashima Kenji, et al. Combined multiphoton imaging and biaxial tissue extension for quantitative analysis of geometric fiber organization in human reticular dermis. Sci Rep 2019;9(1):1–12.

[35] Wang Y, Son S, Swartz SM, Goulbourne NC. A mixed von Mises distribution for modeling soft biological tissues with two distributed fiber properties. Int J Solids Struct 2012;49(21):2914–23.
[36] Jett Samuel V, Hudson Luke T, Baumwart Ryan, Bohnstedt Bradley N, Mir Arshid, Burkhart Harold M, et al. Integration of polarized spatial frequency domain imaging (psfdi) with a biaxial mechanical testing system for quantification of load-dependent collagen architecture in soft collagenous tissues. Acta Biomater 2020;102:149–68.
[37] Zhang Bin, Chester Shawn A, Nadimpalli Siva PV, Suriano Justin T, Theis David P, Lieber Samuel C. Mechanical characterization of porcine skin starting material. J Eng Sci Med Diagn Ther 07 2021;4(4):041002. https://doi.org/10.1115/1.4051563.
[38] Rezakhaniha R, Agianniotis A, Schrauwen JTC, Griffa A, Sage D, Bouten CVC, et al. Experimental investigation of collagen waviness and orientation in the arterial adventitia using confocal laser scanning microscopy. Biomech Model Mechanobiol 2012;11(3–4):461–73. https://doi.org/10.1007/s10237-011-0325-z. ISSN 16177959.
[39] Hwang Jee-hyun, Jeong Haengdueng, Lee Nahyun, Hur Sumin, Lee Nakyum, Han Jeong Jun, et al. Ex vivo live full-thickness porcine skin model as a versatile in vitro testing method for skin barrier research. Int J Mol Sci 2021;22(2):657.
[40] Kuo Ting-Yung, Huang Chao-Cheng, Shieh Shyh-Jou, Wang Yu-Bin, Lin Ming-Jen, Wu Ming-Che, et al. Skin wound healing assessment via an optimized wound array model in miniature pigs. Sci Rep 2022;12(1):1–15.
[41] Otali Dennis, He Qinghua, Grizzle William E. The effect of antigen retrieval on cells fixed in 10% neutral buffered formalin followed by transfer to 70% ethanol. PLoS ONE 2013;8(12):e82405.
[42] Lattouf Raed, Younes Ronald, Lutomski Didier, Naaman Nada, Godeau Gaston, Senni Karim, et al. Picrosirius red staining: a useful tool to appraise collagen networks in normal and pathological tissues. J Histochem Cytochem 2014;62(10):751–8.
[43] O'Brien Kathryn, Bhatia Ayesha, Tsen Fred, Chen Mei, Wong Alex K, Woodley David T, et al. Identification of the critical therapeutic entity in secreted hsp90α that promotes wound healing in newly re-standardized healthy and diabetic pig models. PLoS ONE 2014;9(12):e113956.
[44] Hillman H. Limitations of clinical and biological histology. Med Hypotheses 2000;54(4):553–64.
[45] Cox HT. The cleavage lines of the skin. J Br Surg 1941;29(114):234–40.
[46] Flint Michael H. The biological basis of langer's lines. In: The ultrastructure of collagen; 1976. p. 132–40.
[47] Langer Karl. On the anatomy and physiology of the skin 1. The cleavability of the cutis. Br J Plast Surg 1978;31:3–8.
[48] Wakuri H, Kawamura K, Mutoh K-I. Anatomical observations on cleavage line patterns of the skin in adult pigs. Okajimas Folia Anat Jpn 1993;70(4):181–93.
[49] Wakuri H, Liu J, Chen Y, Mutoh K-I. Developmental-anatomical observations on cleavage line patterns of the skin in Chinese miniature pigs. Okajimas Folia Anat Jpn 1996;72(6):307–16.